JBIC Journal of Biological Inorganic Chemistry (2022) 27:345–355
https://doi.org/10.1007/s00775-022-01928-5

ORIGINAL PAPER

Stability of the H-cluster under whole-cell conditions—formation of an H_{trans}-like state and its reactivity towards oxygen

Marco Lorenzi[1] · Pierre Ceccaldi[1,2] · Patricia Rodríguez-Maciá[3,4] · Holly Jayne Redman[1] · Afridi Zamader[1,5] · James A. Birrell[3] · Livia S. Mészáros[1] · Gustav Berggren[1]

Received: 20 September 2021 / Accepted: 3 January 2022 / Published online: 8 March 2022

Abstract

Hydrogenases are metalloenzymes that catalyze the reversible oxidation of molecular hydrogen into protons and electrons. For this purpose, [FeFe]-hydrogenases utilize a hexanuclear iron cofactor, the H-cluster. This biologically unique cofactor provides the enzyme with outstanding catalytic activities, but it is also highly oxygen sensitive. Under in vitro conditions, oxygen stable forms of the H-cluster denoted H_{trans} and H_{inact} can be generated via treatment with sulfide under oxidizing conditions. Herein, we show that an H_{trans}-like species forms spontaneously under intracellular conditions on a time scale of hours, concurrent with the cells ceasing H_2 production. Addition of cysteine or sulfide during the maturation promotes the formation of this H-cluster state. Moreover, it is found that formation of the observed H_{trans}-like species is influenced by both steric factors and proton transfer, underscoring the importance of outer coordination sphere effects on H-cluster reactivity.

Graphical abstract

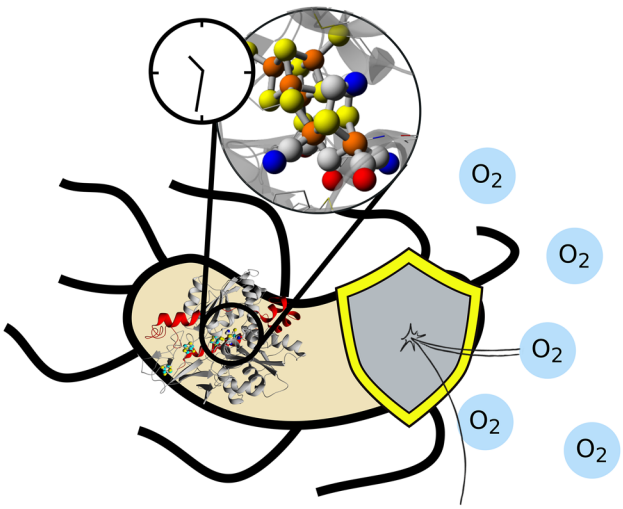

Keywords Metalloenzymes · Hydrogenase · Enzyme mechanism · Electron paramagnetic resonance (EPR) · Biophysics

Introduction

Hydrogen gas (H_2) is a promising energy vector for the coming energy transition, due to its high energy/mass ratio and clean combustion [1, 2]. As of today, the lack of a cheap and efficient catalyst for H_2 production prevents any

✉ Gustav Berggren
Gustav.Berggren@kemi.uu.se

Extended author information available on the last page of the article

possible large-scale application, since currently available technologies all rely on rare or precious elements [3–6]. [FeFe]-hydrogenases (Fig. 1A) are central to hydrogen metabolism in many microorganisms, as they catalyze both H_2 oxidation and evolution [7]. Since their H_2 evolution rates are as high as 10,000 s^{-1}, these enzymes are also highly relevant in the context of developing sustainable biological and bio-inspired synthetic systems for H_2/H^+ interconversion [1, 2, 8–11]. The active site of [FeFe]-hydrogenases (the H-cluster, Fig. 1B) contains a unique diiron subcluster ($[2Fe]_H$) where the low valent Fe ions are bridged by a bidentate azadithiolate ligand ($^-SCH_2NHCH_2S^-$, adt) and further coordinated by three CO and two CN^- ligands [2, 12–15]. The $[2Fe]_H$ subsite is, in turn, attached to a canonical [4Fe-4S] cluster ($[4Fe\text{-}4S]_H$) through a cysteine residue. The ligand geometry of the H-cluster leaves an open-coordination site on the $[2Fe]_H$ subsite positioned in close proximity to the nitrogen of the adt ligand, and the latter is believed to act as a proton relay during catalysis. [FeFe]-hydrogenases are extremely O_2 sensitive enzymes, and this sensitivity represents a key challenge for technological development. The precise inactivation mechanism is still under debate, but O_2 is, with few exceptions, an irreversible inhibitor of the enzyme [16–21]. However, it is possible to protect the H-cluster by forming a reversibly inhibited state, as first observed already in the 1980s in the [FeFe]-hydrogenases from sulfate reducing bacteria including *Desulfovibrio vulgaris* and *Desulfovibrio desulfuricans* (*Dv*HydAB and *Dd*HydAB, respectively, whose protein sequences are identical), following isolation of the enzymes under aerobic conditions [22–25]. The chemical nature of this O_2 stable form has since then been characterized in-depth under in vitro conditions [20, 26–30]. The catalytically active, but O_2 sensitive, H_{ox} state has been observed in all [FeFe]-hydrogenases studied so far, and it exhibits an $[Fe(II)Fe(I)]_H$ subsite while the $[4Fe\text{-}4S]_H$-cluster resides in the oxidized (2 +) state [2, 9, 13, 27] (Fig. 1B). The H_{ox} state is also well-known for its affinity for CO, generating the reversibly inhibited H_{ox}-CO state [31, 32]. In *Dd*HydAB the coordination of a sulfide ligand (SH^-) to the $[2Fe]_H$ subsite converts H_{ox} into the isoelectronic H_{trans} state ($[4Fe\text{-}4S]_H^+$-$[Fe(II)Fe(II)\text{-}SH]_H$), which instead of degrading upon O_2 exposure is oxidized to the so-called H_{inact} state ($[4Fe\text{-}4S]_H^{2+}$-$[Fe(II)Fe(II)\text{-}SH]_H$), also referred to as H_{ox}^{air} [33, 34] (Fig. 1B). Albeit an inhibited state, the H_{inact} state is readily reactivated following release of the sulfide ligand under reducing conditions [19, 27, 29, 35].

Despite having been widely studied in purified form, our insight into the catalytic cycle and stability of [FeFe]-hydrogenases in a cellular environment remains limited. Improved understanding of [FeFe]-hydrogenase reactivity under whole-cell conditions is critical not only to verify the physiological relevance of states observed in vitro, but also to improve the performance of hydrogenase-based biological and biohybrid energy applications. Herein, we take advantage of our capacity to generate semi-synthetic [FeFe]-hydrogenases in *E. coli* at concentrations suitable for whole-cell spectroscopy [9, 36–38], to investigate the formation of the H_{trans} and H_{inact} states under intracellular conditions. More specifically, we explore two different model enzymes: HydA1 from the green algae *Chlamydomonas reinhardtii* (*Cr*HydA1) and the aforementioned bacterial *Dd*HydAB. Moreover, a recent mechanistic proposal underscores the need for efficient proton-transfer during the formation of these sulfide-inhibited states [34]. Thus, we probe the influence of sterics and the proton-transfer network on the inhibition chemistry of the *Cr*HydA1 enzyme, through modifications of the organometallic cofactor as well as single-point mutations in the active-site pocket.

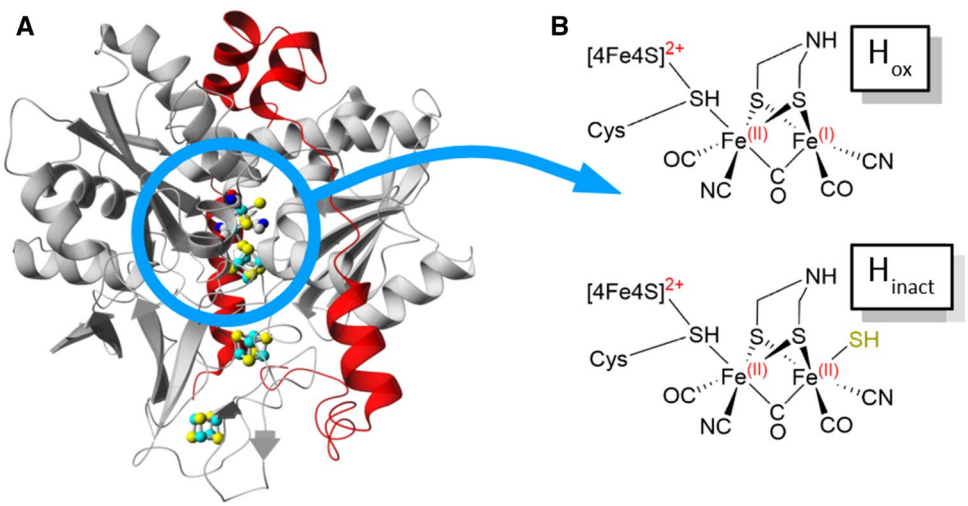

Fig. 1 Schematic representation of [FeFe]-hydrogenase and the H-cluster. **A** The dimeric *Desulfovibrio desulfuricans* [FeFe]-hydrogenase (*Dd*HydAB) in the H_{inact} state, based on the crystal structure reported in ref [33] (PDB ascension number 6SG2). Subunit A is colored in gray, subunit B is colored in red, the color scheme for the H-cluster and for the accessory [FeS] clusters is based on the elements (Fe: cyan; S: yellow; N: blue; O: red; C: gray). **B** The H-cluster in the catalytically active state H_{ox} and in the inhibited state H_{inact}

Results and discussion

Formation of an H_{trans}-like state under whole-cell conditions

To generate enzyme concentrations enabling H-cluster detection by electron paramagnetic resonance (EPR) spectroscopy *Cr*HydA1 was heterologously expressed in standard *E.coli* BL21, as previously described [36–39]. As *E. coli* does not natively express an [FeFe]-hydrogenase, the organism lacks the [FeFe]-hydrogenase-specific accessory proteins (HydEFG) and produces the enzyme in an inactive form, complete with the $[4Fe\text{-}4S]_H$ cluster but lacking the diiron $[2Fe]_H$ cofactor (*apo-Cr*HydA1) [40–42]. After protein overproduction, cell cultures were concentrated and the active semi-synthetic enzyme (holo-*Cr*HydA1, herein denoted $[2Fe]^{adt}$-*Cr*HydA1) was subsequently generated through the addition of the synthetic $[2Fe]_H$ cofactor mimic $[Fe_2(adt)(CO)_4(CN)_2]^{2-}$ ($[2Fe]^{adt}$) under strictly anaerobic conditions. The final concentration of $[2Fe]^{adt}$ in the cell suspension was 80 µM, as this has previously been shown to afford close to quantitative maturation of apo-*Cr*HydA1 under these conditions [36–39, 43]. The cell suspensions produced H_2 for 1–2 h following the addition of $[2Fe]^{adt}$, before slowing down significantly and halting production after 3–4 h (Fig. S1). In parallel to quantifying H_2 production, whole-cell samples for EPR analysis were collected and flash frozen at different time points to monitor the formation and stability of the $[2Fe]^{adt}$-*Cr*HydA1 holoenzyme over the course of 23 h. EPR spectra recorded on samples obtained after a 20 min incubation with $[2Fe]^{adt}$ under an argon atmosphere displayed a mixture of one rhombic ($g_z \neq g_y \neq g_x$) and one pseudo-axial ($g_x = g_y \neq g_z$) feature, respectively attributable to the H_{ox} ($g_{zyx} = 2.100, 2.040, 1.998$) and to the CO-inhibited H_{ox}-CO states ($g_{\parallel\perp} = 2.054, 2.007$) [31] (Fig. 2). The H_{ox} and H_{ox}-CO species continued to be the main constituents of the signal over the first 3 h, with the latter species gradually releasing CO and converting into the H_{ox} state. (Fig. 2B).

However, after 23 h of incubation, a significant decrease in the features specific to these two states is observed, concomitantly with the rise of a relatively broad rhombic signal with $g_{zyx} = 2.064, 1.972, 1.910$. Simulations show that the latter species begins to form already after 2 h of incubation, at which point it represents ~ 10% of the total spin count. This rhombic signal accumulates with time to then become the dominant species in the sample, contributing for ~ 80% of the total signal intensity after 23 h. At this point, the cells are able to resume H_2 production when re-suspended in fresh media containing glucose (Fig. S1); however, the

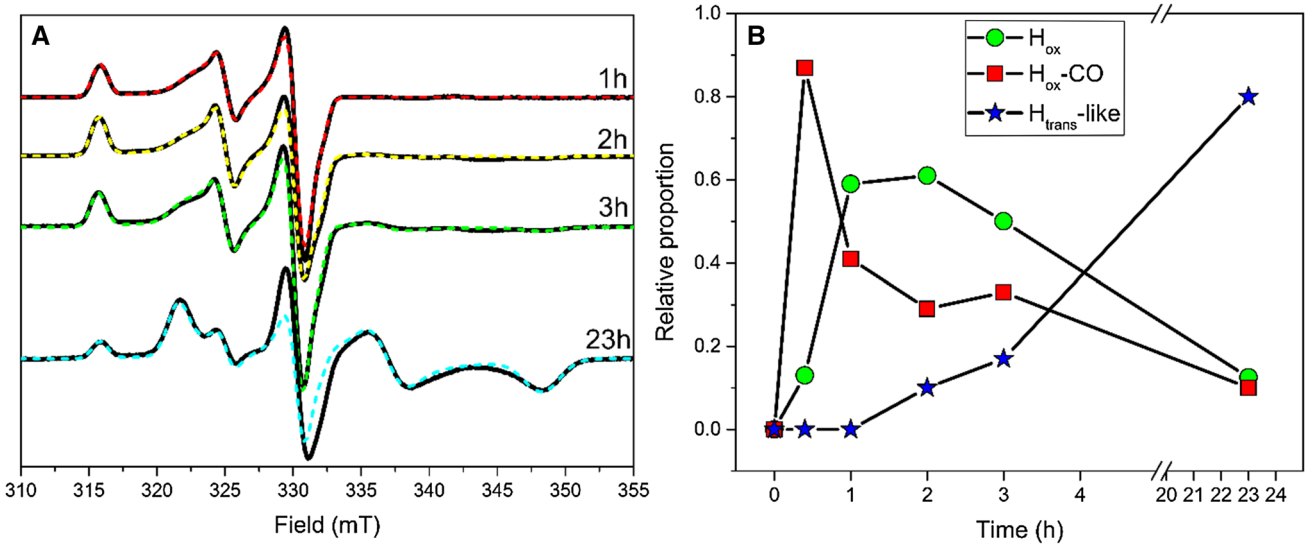

Fig. 2 The effect of time on the population of H-cluster states in $[2Fe]^{adt}$-*Cr*HydA1 monitored by EPR spectroscopy. **A** Whole-cell EPR spectra of $[2Fe]^{adt}$-*Cr*HydA1 recorded on samples of *E. coli* cells expressing *apo-Cr*HydA1 and flash frozen following incubation with the $[2Fe]^{adt}$ cofactor for 1 h, 2 h, 3 h and 23 h at 37 ˚C under anaerobic conditions. Experimental spectra from a representative dataset are overlaid with simulations (dashed lines), including H_{ox}, H_{ox}-CO and H_{trans} contributions. All spectra were corrected by subtracting the *apo-Cr*HydA1 control sample, to eliminate any signal coming from the cells and from unmatured *Cr*HydA1 (Fig. S4). The poor fitting around 330 mT on the 23 h spectrum is due to the imperfect subtraction of the variable $g = 2.02$ isotropic signal arising from the cell background, which is a minor contribution in the difference spectrum (see Fig. S4). EPR experimental conditions: T = 20 K, P = 1 mW, $\nu = 9.28$ GHz. **B** Contribution of the different catalytic states to the signal intensity at the different time points on the same dataset. The relative contributions are calculated based on their respective weight in the simulations

media exchange has no effect on the relative proportion of the different states (Fig. S2). Similarly, the broad rhombic signal displayed negligible changes when parallel samples incubated for 23 h were exposed to strongly reducing conditions via the addition of sodium dithionite and 1 atm H_2 (data not shown). In combination, these observations suggest that, once formed, the species giving rise to the rhombic signal is highly stable. Thus, the H_2 produced by aged cells is attributed to the small residual population still residing in the catalytically competent H_{ox} state.

The broad rhombic EPR signal ($g_{zyx} = 2.064$, 1.972, 1.910) was not observed when cells expressing apo-*Cr*HydA1 were incubated for up to 23 h in the absence of $[2Fe]^{adt}$, nor in standard BL21 cells incubated with the same complex (Fig. S3), supporting the assignment of the signal to an H-cluster species. The g values of this new broad EPR signal are in good agreement with a signal previously attributed to the sulfide-inhibited H_{trans} state in *Dd*HydAB ($g_{zyx} = 2.060$; 1.960; 1.890) [25, 29]. To assess whether the origin of this new signal could be attributed to the binding of a sulfide or hydrosulfide ligand to the diiron subcluster, 375 µM Na_2S were added to the incubation mixture concomitantly with $[2Fe]^{adt}$. The addition of sulfide increased the overall intensity of the rhombic H_{trans}-like signal, as reported for the in vitro formation of the H_{trans} state in *Dd*HydAB [34]. The same effect could be observed using L-cysteine as the source for the sulfide, albeit with a lower magnitude (Fig. S5).

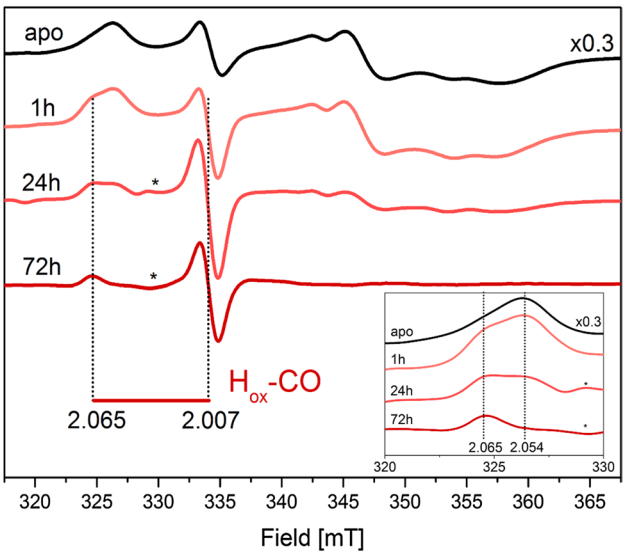

Fig. 3 The effect of time on the population of H-cluster states in $[2Fe]^{adt}$-*Dd*HydAB monitored by EPR spectroscopy. Whole-cell EPR spectra of apo- and $[2Fe]^{adt}$-*Dd*HydAB recorded on samples of *E. coli* cells expressing apo-*Dd*HydAB and flash frozen prior to or following incubation with the $[2Fe]^{adt}$ cofactor for 1 h, 24 h and 72 h under anaerobic conditions at 37 °C. The figure reports the g values for the H_{ox}-CO state. (Inset): zoom in on the 320–330 mT area. Vertical dotted lines indicate the g = 2.065 feature belonging to H_{ox}-CO and the g = 2.054 from the [4Fe-4S] clusters interaction spectrum. Asterisks mark a feature attributable to the $(F_{red})H_{ox}$ interaction spectrum. EPR experimental conditions: T = 20 K, P = 1 mW, ν = 9.28 GHz. Note that the spectrum of apo-*Dd*HydAB has been normalized by a factor 0.3

Intracellular H_{trans} formation in *Dd*HydAB

The heterodimeric *Dd*HydAB hydrogenase has been the primary model system for elucidating the chemistry of the H_{trans} and H_{inact} states [29, 33, 34]. Thus, this enzyme was also studied under intracellular conditions for comparative purposes, with *Dd*HydAB overproduced in *E. coli* using the same methods as for *Cr*HydA1. In addition to the $[4Fe\text{-}4S]_H$ component of the H-cluster, *Dd*HydAB features two additional [4Fe-4S] "F-clusters" serving as electron relays from the protein surface to the active site (Fig. 1A). The apo-*Dd*HydAB protein, containing only the three [4Fe-4S] clusters, shows an interaction spectrum of the [4Fe-4S] clusters' signals under intracellular conditions (Fig. 3, apo-*Dd*HAB), as observed earlier for the purified enzyme [44]. In vitro activation of *apo-Dd*HydAB using $[2Fe]^{adt}$ to generate $[2Fe]^{adt}$-*Dd*HydAB (i.e. *holo-Dd*HydAB) is a relatively slow process. The mechanistic rationale for this remains to be elucidated, but is arguably attributable to the relative stabilities of the so-called "open" and "closed" conformations of the enzyme [44]. Nevertheless, treating apo-*Dd*HydAB expressing *E. coli* cells with $[2Fe]^{adt}$ for just 1 h yielded a complex spectrum, with an axial signature attributable to an H_{ox}-CO species clearly discernible under the dominant [4Fe-4S] interaction spectrum. The reason for the apparent higher rate of H-cluster assembly in *Dd*HydAB under whole-cell conditions is unknown. Extending the incubation time to 24 h resulted in a decrease of the [4Fe-4S] signals, possibly due to gradual oxidation, allowing also for the detection of a contribution arising from a small population of $[2Fe]^{adt}$-*Dd*HydAB featuring the H-cluster in the H_{ox} state and a one-electron-reduced F-cluster (denoted $(F_{red})H_{ox}$) [45]. However, no features attributable to H_{trans} or an H_{trans}-like state were observed, even when extending the incubation time to 72 h, at which point the only remaining H-cluster signal is H_{ox}-CO (Fig. 3). These experiments verify that $[2Fe]^{adt}$-*Dd*HydAB can be generated through artificial maturation under whole-cell conditions, at a seemingly faster rate than during normal in vitro studies. Still, the lack of any H_{trans}-like species in the case of *Dd*HydAB shows that the stability of this state under intracellular conditions can vary significantly between different [FeFe]-hydrogenases, as expected from variations in structure as well as reported affinities for other inhibitors such as carbon monoxide [46].

Reactivity of the H_{trans}-like state towards molecular oxygen.

As mentioned in the introduction, in *Dd*HydAB the H_{inact} state forms via H_{trans} under oxidative conditions (e.g. during aerobic purification) and has been demonstrated to grant protection from O_2-induced H-cluster degradation. Conversely, *Cr*HydA1 is known to be an extremely oxygen-sensitive enzyme and aerobic purification of an active enzyme has not been reported [20]. Still, *Cr*HydA1 has also been shown to be able to enter the O_2-protected H_{inact} state under controlled in vitro conditions [34]. To examine if exposing whole-cell [2Fe]^{adt}-*Cr*HydA1 samples to molecular oxygen could trigger the formation of H_{inact} or H_{trans}, and whether these states were able to grant resistance towards O_2 damage, cell suspensions were exposed to air and the effects on the H-cluster were monitored via EPR spectroscopy and enzyme activity assays. As described above, incubating cells expressing apo-*Cr*HydA1 with [2Fe]^{adt} for 1 h under anaerobic conditions, generates an enzyme population consisting of H_{ox} and H_{ox}-CO. Subsequent exposure of such samples to O_2, by placing them in air for 1 h, resulted in a noticeable decrease of the overall EPR signal intensity (total residual signal intensity ≈ 45%) (Fig. 4, panel A). Visibly, all of the residual signal is attributable to the H_{ox}-CO state; this is expected as it is known to be more resistant to oxygen and to be formed by CO released upon H-cluster degradation (a process known as "cannibalization") [27, 29]. The same air exposure treatment on samples pre-incubated under argon for 23 h, in which the H-cluster resides primarily in the H_{trans}-like state, yielded a similar result, with a decrease in the intensity of the spectral features of both the H_{trans}-like species and residual H_{ox} (total residual signal intensity ≈ 35%) (Fig. 4, panel B). This loss of EPR signal intensity can be attributed either to the formation of an EPR silent H_{inact}-like state or to O_2-induced degradation of the H-cluster. To separate these two possibilities, the EPR experiments were complemented with in vitro activity assays on lysed cells. The use of a strong reductant (dithionite), in combination with methyl viologen as electron mediator, is expected to re-activate any H-cluster fraction residing in H_{inact} or H_{trans}, and thus enable quantification of the entire intact H-cluster population.

It should be noted that already prior to O_2 exposure the 23 h pre-incubated samples did display slightly diminished activities, as compared to the 1 h pre-incubated samples (compare Fig. 4A and B, insets). We attribute this to H-cluster degradation, as in vitro assays show no indication of degradation processes involving the protein scaffold on a 24 h time scale (Fig. S4). The readily observable H_2 production from the lysed cells enable a relative quantification of intact enzyme to determine the effect of O_2 on the different preparations. Regardless of pre-incubation time (1 or 23 h), the signal loss observed by EPR spectroscopy following oxygen

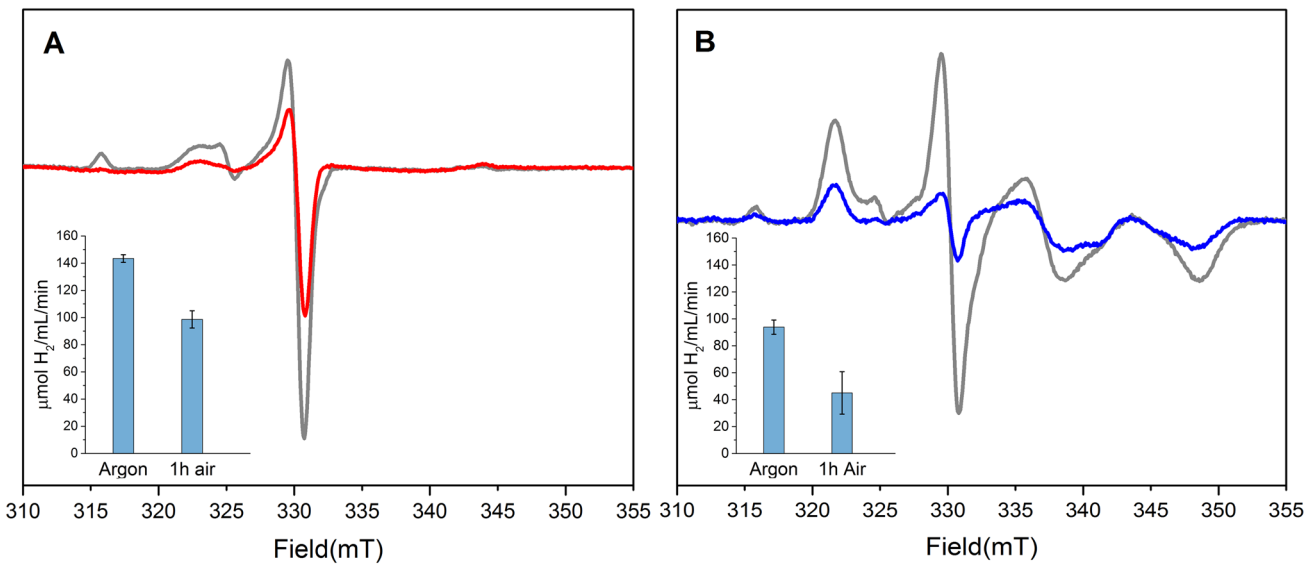

Fig. 4 Reactivity towards molecular oxygen of whole-cell [2Fe]^{adt}-*Cr*HydA1 samples. **Panel A:** The EPR spectrum of a whole-cell [2Fe]^{adt}-*Cr*HydA1 sample initially incubated for 1 h with [2Fe]^{adt} under anaerobic conditions, and subsequently exposed to air for 1 h **(red spectrum)** is overlaid with an equivalent sample kept strictly anaerobic **(gray spectrum).** (**Inset**): Enzymatic activities for the same samples measured through in vitro assays. **Panel B:** The EPR spectrum of a whole-cell [2Fe]^{adt}-*Cr*HydA1 sample initially incubated for 23 h with [2Fe]^{adt} under anaerobic conditions, and subsequently exposed to air for 1 h at ambient temperature **(blue spectrum)** is overlaid with an equivalent sample kept anaerobic **(gray spectrum).** (**Inset**): Enzymatic activities for the same samples measured through in vitro assays. EPR data shown come from representative spectra. Activity data represent the average values of two biological replicates with standard deviations reported as error bars. EPR experimental conditions: T = 20 K, P = 1 mW, ν = 9.28 GHz

exposure was larger than the activity loss. The 1 h-pre-incubated sample retained ~ 70% of the H_2-producing activity and the 23 h-pre-incubated sample retained ~ 50% of its activity, when compared to parallel samples kept under strictly anaerobic conditions (Fig. 4, insets).

Consequently, the observed EPR signal loss is attributable to a combination of H-cluster degradation and formation of an EPR silent H_{inact}-like state. Considering the well-established reactivation of H_{inact} under reducing conditions [29, 34], we expect the latter species to re-enter the catalytic cycle under the conditions employed in the in vitro activity assays, while the former causes a definitive loss in activity. Moreover, pre-established accumulation of the H_{trans}-like state did not provide any apparent increase in O_2-tolerance, as samples pre-incubated for 23 h showed larger relative activity losses as compared to samples pre-incubated only for 1 h. In contrast, the cellular environment showed remarkable capabilities in terms of O_2-protection, as a significant fraction of the H-cluster population was not degraded nor oxidized to an H_{inact}-like state during oxygen exposure. This is attributed to the low intracellular O_2 concentrations ensured by cellular respiration, a process which is indeed expected to be more efficient in "young" and metabolically active cells [47].

Structural factors influencing formation of the H_{trans} and H_{inact}-like states

The presence of an efficient proton-transfer chain has been proposed to be important for the formation of the H_{trans} and H_{inact} states, as the sulfide ligand is thought to enter the active-site pocket as H_2S and to undergo a protein-assisted deprotonation event to yield the SH^- ligand [34]. Thus, modifications were made to both the $[2Fe]_H$ subsite as well as to the active-site pocket to assess the importance of the proton-transfer pathway on formation of the H_{trans} and H_{inact}-like states. More specifically, holo-*Cr*HydA1 samples were prepared in which the $[2Fe]^{adt}$ mimic was replaced with $[Fe_2(pdt)(CO)_4(CN)_2]^{2-}$ ($[2Fe]^{pdt}$, pdt = $^-SCH_2CH_2CH_2S^-$, propanedithiolate), generating $[2Fe]^{pdt}$–*Cr*HydA1. In this modified H-cluster, the amine bridgehead present in the natural $[2Fe]^{adt}$ cofactor is substituted with a non-protonatable methylene group. Earlier whole-cell and in vitro spectroscopic studies, as well as crystallographic studies, have shown that $[2Fe]^{pdt}$–*Cr*HydA1 is an organometallic variant where the [2Fe] subsite is locked in an oxidized Fe(II) Fe(I) state, strikingly similar to the EPR active H_{ox} state of the native enzyme [14, 37–39, 43, 48, 49]. As expected, EPR samples consisting of apo-*Cr*HydA1-expressing cells incubated with the $[2Fe]^{pdt}$ complex revealed the exclusive formation an H_{ox}-like species. The H-cluster population remained locked in the H_{ox} state for up to 23 h of incubation under anaerobic conditions; and no features attributable to an H_{trans}-like species were discernable at any point during the experiment (Fig. S6).

These results seem to confirm the importance of a proton relay in the second coordination sphere of the H-cluster for the formation of the H_{trans} and H_{inact}-like states. To proceed one step further down the proton-transfer pathway, the C169 residue was mutated to a serine (*Cr*HydA1-C169S). This cysteine residue is strictly conserved in "prototypical" [FeFe]-hydrogenases, and it is the first amino acid involved in the proton-transfer chain towards the adt-nitrogen of the H-cluster [9]. The C169S mutant has been studied extensively under in vitro conditions, and demonstrated to be a variant with a severely compromised proton-transfer pathway and significantly decreased catalytic activity [50, 51]. Incubating *E. coli* cells expressing *Cr*HydA1-C169S with $[2Fe]^{adt}$ resulted in the rapid formation of a broad rhombic EPR signal with g_{zyx} = 2.064; 1.970; 1.910, very closely matching the H_{trans}-like signal in the wild-type enzyme (g_{zyx} = 2.064; 1.972; 1.910). A signal with comparable EPR properties has been reported from in vitro studies of the C169S mutant (g_{zyx} = 2.065; 1.969; 1.906) [51, 52]. It was originally assigned to an H_{trans}-like species, potentially featuring a hydride ligand. However, despite the similarity in g values the signal observed under our in vivo conditions is highly unlikely to represent a metal hydride species. No other H-cluster derived features were discernable in the EPR spectrum (Fig. 5).

The evolution of this H_{trans}-like signal over time was examined with long-term (1 h, 3 h, 23 h, 48 h) incubation of the cells with the $[2Fe]^{adt}$ cofactor, and no significant change was detected neither in the shape, nor intensity of the signal (Fig. 5). The stability of this state was further confirmed by its isolation. In contrast to the wild-type protein, $[2Fe]^{adt}$-*Cr*HydA1-C169S could be purified in its H_{trans}-like state via affinity chromatography following anaerobic cell lysis. However, this required supplementing the buffers with 100 mM Na_2S, as omitting sulfide resulted in a complete loss of the H_{trans}-like rhombic EPR signal (Fig. S7). Albeit EPR spectroscopy revealed rapid H-cluster formation, no in vivo or in vitro hydrogen production could be detected from $[2Fe]^{adt}$-*Cr*HydA1-C169S samples, as expected from this reportedly inactive variant [50].

To gain more insight into potential intermediates formed on route to the H_{trans}-like state in the C169S mutant, the process was studied at lower temperature. More specifically, apo-*Cr*HydA1-C169S containing cells were treated with $[2Fe]^{adt}$ at 12 °C. The first discernable state generated under these conditions was H_{ox} (20–60 min), while the H_{trans}-like state only started to be detectable after 2 h of incubation with $[2Fe]^{adt}$ (Fig. S8). The H_{trans}-like signal reached full intensity after overnight incubation with the cofactor.

As modifications of the bridgehead atom showed clearly diverging effects as compared to the C169S mutant, with

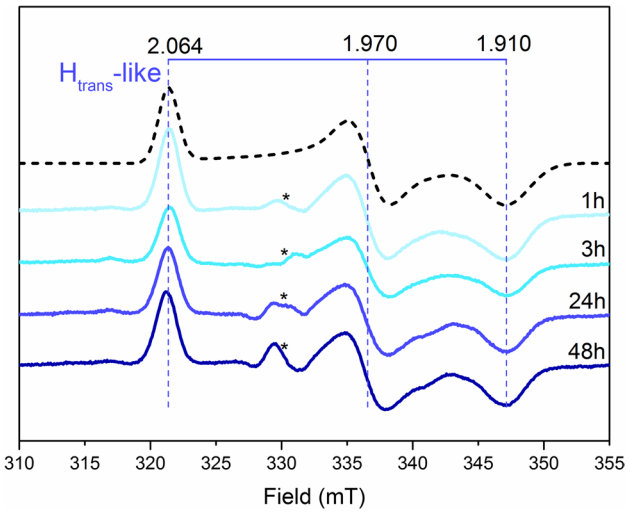

Fig. 5 Monitoring the formation of the H_{trans}-like state in $[2Fe]^{adt}$-*Cr*HydA1-C169S under whole-cell conditions by EPR spectroscopy. EPR spectra recorded for *E. coli* cells expressing apo-*Cr*HydA1-C169S flash frozen after incubation with $[2Fe]^{adt}$ for 1, 3, 24 or 48 h at 37 °C. A characteristic H_{trans}-like signature became visible already after 1 h of incubation; a spectral simulation for this species is shown as a stacked dashed line and g values obtained from the fittings are reported. Unassigned, sample-specific weak signals potentially arising from the imperfect subtraction of the cell background are indicated with asterisks. EPR experimental conditions: T = 20 K, P = 1 mW, ν = 9.28 GHz

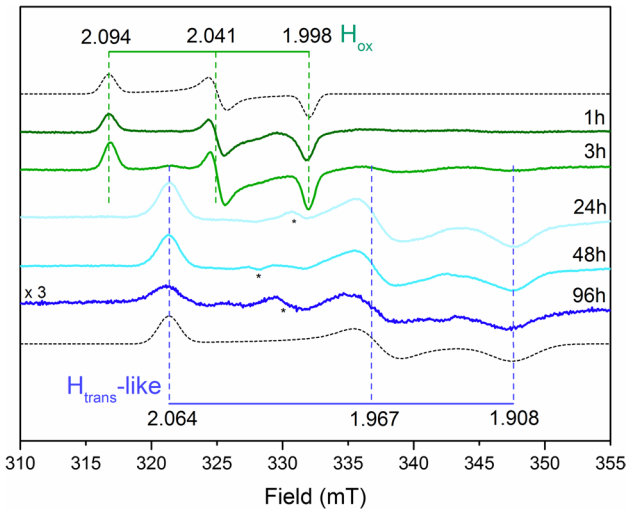

Fig. 6 Monitoring the formation of the H_{trans}-like state in *Cr*HydA1-C169S with the $[2Fe]^{pdt}$ cofactor. EPR spectra of *E. coli* cells expressing apo-*Cr*HydA1-C169S after incubation with $[2Fe]^{pdt}$ for variable amounts of time at 37 °C. The H_{trans}-like signature only became visible after 23 h of incubation. Unassigned, sample-specific weak signals potentially arising from the imperfect subtraction of the cell background are indicated with asterisks. EPR experimental conditions: T = 20 K, P = 1 mW, ν = 9.28 GHz

regards to formation of the H_{trans}-like state, the combined effect of the latter mutation and the methylene-bridgehead mimic was investigated. Whole-cell samples of the C169S mutant matured with $[2Fe]^{pdt}$ ($[2Fe]^{pdt}$-*Cr*HydA1-C169S) initially displayed a behavior consistent with the $[2Fe]^{pdt}$ wild-type, with an EPR spectrum showing an H-cluster apparently locked in an H_{ox}- like state (Fig. 6). However, a signal corresponding to an H_{trans}-like state started to accumulate after 3 h of incubation and became predominant after 24 h. No other signals arose thereafter, on a time scale of days (96 h).

In summary, the $[2Fe]^{pdt}$-variant of the wild-type *Cr*HydA1 does not form detectable amounts of any H_{trans} or H_{inact}-like states, in agreement with previous studies performed in vitro [34]. Conversely, the $[2Fe]^{pdt}$-*Cr*HydA1-C169S 'double' variant showed accumulation of the H_{trans}-like state. This shows that the presence of a nitrogen-bridgehead facilitates, but is not critical, for the formation of these inhibited states. Rather, it underscores that additional factors in the outer coordination sphere also affect their formation. These include a decrease of steric bulk resulting from the replacement of a thiol group with an alcohol that provides easier access for exogenous ligands and a change in the hydrogen-bonding dynamics involving the first and second coordination spheres.

Conclusions

Semi-synthetic [FeFe]-hydrogenases have been shown to remain catalytically active in cyanobacteria on a time scale of days [43, 53]. The observation that *E. coli* cells expressing *C. reinhardtii* [FeFe]-hydrogenase can produce hydrogen gas only transiently following enzyme activation has raised the question on the stability of these enzymes in the bacterial cytoplasm.

In the case of *Cr*HydA1, EPR spectra recorded on long time-scale samples show the gradual accumulation of an H_{trans}-like state under the slow-turnover conditions assayed here. However, the rate of formation of this H_{trans}-like state clearly varies between [FeFe]-hydrogenases, as *Dd*HydAB did not form a similar state under identical experimental conditions. The latter observation is tentatively attributed to *Dd*HydAB's high affinity for CO, resulting in a relatively stable H_{ox}-CO population unable to convert to the H_{trans}-like state under the conditions employed here.

In light of its stability, we propose that the observed H_{trans}-like state represents a thermodynamic sink for the enzyme accessed under the whole-cell conditions employed here. Moreover, its formation is evidently accelerated by mutating amino-acid residues close to the open-coordination site of the cofactor, and by the presence of an amino-group in the bridging dithiolate ligand. Models have been proposed that focus on the role of the hydrogen-bonding network in stabilizing apical ligands, therefore, it can be

hypothesized that the nature of the H-bond partners in the vicinity of the apical site can significantly influence the formation of an inhibited state. [54] In addition, a cysteine-to-serine mutation has the effect of reducing the steric hindrance close to the open-coordination site of the cofactor, which could further facilitate the insertion of an inhibitor ligand. The positive effect of adding sulfide for generating this species and stabilizing it, as during isolation of [2Fe]^{adt}-*Cr*HydA1-C169S, suggests that the observed rhombic EPR signal can be attributed to the in vitro characterized H_{trans} state. The observation of H_{trans} under whole-cell conditions would support a physiological relevance of this state. However, we note that the in vivo data does not unequivocally prove the structure of this species, and further investigations on the nature of this H_{trans}-like state are underway.

Albeit the H_{trans}-like state appears stable, it does not seem to offer substantial protection against oxygen damage, in contrast to in vitro observations [33, 34]. Conversely, *E. coli* cells were found to provide a surprisingly high level of protection versus air, highlighting the potential of *E. coli* as a suitable host organism for oxygen-sensitive enzymes in bio (hybrid) technological applications.

In closing, the spontaneous formation of inactive species could pose a problem in the development of systems that take advantage of bacterial hosts to develop whole-cell hydrogen production systems, as it potentially shortens their service life. Having discovered the critical role of the steric occupancy and the hydrogen-bonding network of the active-site pocket in regulating the kinetics of this phenomenon, a possible path for research could be to fine-tune these parameters and thus develop potentially more robust catalysts.

Experimental procedures

General. All chemicals were purchased from Sigma-Aldrich or VWR and used as received unless otherwise stated. All anaerobic work was performed in an MBRAUN glovebox ($[O_2] < 10$ ppm). The expression vector encoding the *hydA1* gene (pETDuet-*Cr*HydA1-His) was kindly provided by Prof. Marc Fontecave (College de France, Paris/CEA, Grenoble). $(Et_4N)_2[Fe_2(adt)(CO)_4(CN)_2]$ ([2Fe]^{adt}]) and $(Et_4N)_2[Fe_2(pdt)(CO)_4(CN)_2]$ ([2Fe]^{pdt}]) were synthesized in accordance to literature protocols with minor modifications, and verified by FTIR spectroscopy [55–58]. The complexes were dissolved in anaerobic potassium phosphate buffer (100 mM, pH 6.8) at 10 µg/µL concentration and used directly. Protein content was analyzed by 10% SDS-PAGE minigels in a BioRad Mini-PROTEAN Tetra Cell system. Protein bands were stained with Page Blue protein staining solution (Thermo Fisher Scientific) according to the supplier`s instructions.

Generation of *Cr*HydA1-C169S mutant. To generate the C169S mutant in HydA1 protein, the triplet coding for the cysteine amino acid in position 169 (TGC) was replaced with one coding for serine (TCC). The pETDuet-*Cr*HydA1-His was mutated with the Quick Change Site-Directed Mutagenesis Kit (Agilent) according to the manufacturer instructions using 5` GTTTACCAGCTCCTGCCCGGG CTGGATTGC` 3` and 5` GCAATCCAGCCCGGGCAG GAGCTGGTAAAC` 3` primers. The amino-acid change was verified by sequencing.

Overexpression of the apo-*Cr*HydA1 hydrogenase. *Escherichia coli* BL21(DE3) cells containing the *Cr*HydA1 plasmid were grown in 50 mL M9 medium [22 mM Na_2HPO_4, 22 mM KH_2PO_4, 85 mM NaCl, 18 mM NH_4Cl, 0.2 mM $MgSO_4$, 0.1 mM $CaCl_2$, 0.4% (v/v) glucose] under aerobic conditions until $O.D._{600} = 0.6 – 0.8$ in the presence of ampicillin. The protein overproduction was induced with 1 mM IPTG and persisted at 20 °C for 16 – 18 h with continuous aeration. The media was supplemented with 100 µM $FeSO_4$ at the time of the induction. Final $O.D._{600}$ of the cultures were 1.4 ± 0.2.

Overexpression of the apo-*Dd*HydAB hydrogenase. *Escherichia coli* BL21(DE3) cells containing the pACYCDuet-*Dd*HydAB plasmid[44] were grown in 50 mL M9 medium [22 mM Na_2HPO_4, 22 mM KH_2PO_4, 85 mM NaCl, 18 mM NH_4Cl, 0.2 mM $MgSO_4$, 0.1 mM $CaCl_2$], supplemented with 0.4% (w/v) glucose, under aerobic conditions until $O.D._{600} = 0.6 – 0.8$ in the presence of chloramphenicol. The protein overproduction was induced with 1 mM IPTG and persisted at 20 °C for 16–18 h with continuous aeration. The media was supplemented with 400 µM $FeSO_4$ at the time of the induction. Final $O.D._{600}$ of the cultures were 1.4 ± 0.2.

In vivo formation of [2Fe]^{adt}-*Cr*HydA1, [2Fe]^{pdt}-*Cr*HydA1, [2Fe]^{adt}–*Dd*HydAB and [2Fe]^{pdt}-*Dd*HydAB. The preparation of the semi-synthetic hydrogenase was performed following literature protocols with minor modifications [38, 39]. The apo-protein was expressed in 50 mL *E. coli* cultures as described in the "*Overexpression of the apo-CrHydA1 hydrogenase"* and "*Overexpression of the apo-DdHydAB hydrogenase"* sections. After the 16–18 h expression period the cells were harvested, deaerated and transferred to the glovebox. The cells were re-suspended in fresh M9 medium (2 mL final volume), and formation of [2Fe]^{adt}–*Cr*HydA1, [2Fe]^{pdt}–*Cr*HydA1, [2Fe]^{adt}–*Dd*HydAB and [2Fe]^{pdt}-*Dd*HydAB was achieved by incubating the cell suspensions with 100 µg (156 nmol) [2Fe]^{adt} or 100 µg (156 nmol) [2Fe]^{pdt} complex (80 µM final conc.), for 1 – 96 h at 37 ˚C under strictly anaerobic conditions. When indicated, the medium was supplemented with 375 µM L-cysteine or 375 µM Na_2S.

For the medium exchange experiments, after 23 h incubation the cell suspensions were transferred in the

glovebox, centrifuged and the resulting pellet was re-suspended in fresh M9 media, supplemented with 0.4% (w/v) glucose when necessary. The cell suspensions were then incubated for 2 h at 37 ˚C under strictly anaerobic conditions.

Whole-cell EPR sample preparation. The 2 mL concentrated cell suspensions generated via the "In vivo *formation of [2Fe]^{adt}-HydA1, [2Fe]^{pdt}-HydA1, [2Fe]^{adt}–DdHydAB and [2Fe]^{pdt}-DdHydAB*" protocol were centrifuged and the cell pellet washed with 1 mL TRIS–HCl buffer (100 mM TRIS, 150 mM NaCl pH 7.5) three times under anaerobic conditions. After washing, the cells were diluted to a final volume of 400 µL using the same buffer and transferred into EPR tubes. The tubes were capped and directly frozen in liquid nitrogen.

Isolation of [2Fe]^{adt}-*Cr*HydA1-C169S. 100 mL of C169S-*Cr*HydA1 cells were activated with 100 µg [2Fe]^{adt} for 1 h. After activation the cells were lysed in lysis buffer (50 mM sodium phosphate buffer pH 7.8, 100 mM NaCl, 20 µg/mL DNaseI, 40 µg/mL RNaseI, 1 mM $MgCl_2$, 0.1 mg/mL lysozyme) using three freeze–thaw cycles. The soluble fraction of the cell lysate was separated with 13,000 rpm centrifugation for 20 min under anaerobic conditions. The protein was purified using a 1 mL Ni-sepharose High Performance (GE Heathcare) gravity column equilibrated with 10 column volumes of equilibration buffer (50 mM sodium phosphate buffer pH 7.8, 100 mM NaCl) in the glovebox. The non-specifically bound proteins were removed with wash buffer (50 mM sodium phosphate buffer pH 7.8, 100 mM NaCl, 20 mM imidazole). The [2Fe]-C169S-*Cr*HydA1 protein was eluted with 1.5 mL elution buffer (50 mM sodium phosphate buffer pH 7.8, 100 mM NaCl, 300 mM imidazole), the elution fraction was directly used for EPR samples. The purity of the purified protein was confirmed with SDS-PAGE.

Hydrogenase activity measurements. Activity measurements were performed on whole-cell samples as well as under in vitro conditions using published protocols [39]. Selected technical details are re-iterated for clarity. Whole-cell activities were determined from cell suspensions (2 mL final volume), incubated in gastight vials with a total volume of 9 mL. In vitro assays were performed on cell lysates. The reaction mix contained potassium phospate buffer (pH 6.8, 100 mM), Triton-X 1.5% v/v and methyl viologen (14 mM);the reaction was initiated with the addition of dithionite (200 mM) and the sample vials incubated for 15 min at 37 °C prior to headspace sampling. Hydrogen production was determined by analyzing the headspace gas, using a gas chromatograph (GC; PerkinElmer LLC, MA, USA) equipped with a thermal conductivity detector (TCD) and a stainless-steel column packed with Molecular Sieve (60/80 mesh). A calibration curve was established by injecting known amounts of hydrogen. The operational temperatures of the injection port, the oven and the detector were 100 °C, 80 °C and 100 °C, respectively. Argon was used as the carrier gas at a flow rate of 35 mL min^{-1}.

EPR measurements. The EPR spectra shown are representative signals from at least two individual experiments. The individual experiments show some preparation dependent differences, but the amplitude of these background signals are negligible compared to the signal intensity of the [2Fe]^{adt} activated *Cr*HydA1. Measurements were performed on a Bruker ELEXYS E500 spectrometer using an ER049X SuperX microwave bridge in a Bruker SHQ0601 cavity equipped with an Oxford Instruments continuous flow cryostat and using an ITC 503 temperature controller (Oxford Instruments). Measurement temperatures ranged from 10 to 20 K, using liquid helium as coolant, with the following EPR settings unless otherwise stated: microwave power 1 mW, modulation amplitude 1 mT, modulation frequency 100 kHz. The spectrometer was controlled by the Xepr software package (Bruker).

EPR spectra processing and simulations. The EPR spectra were processed using the softwares Matlab (Mathworks, Inc) and QSoas [59]. Matlab served for converting the EPR files to ascii format, while QSoas was used to display the spectra as a function of g values, for visual inspection and subtraction of background signals emerging from the cells. The processed signals were used for Figs. 2, 3, 4, 5, 6, S2 and S3, S5 to S8. The simulations were performed using the Easyspin toolbox (5.2.23) within Matlab [60]. Other details of the procedure can be found in [38].

Supplementary Information The online version contains supplementary material available at https://doi.org/10.1007/s00775-022-01928-5.

Acknowledgements The Horizon 2020 program, European Research Council Starting Grant, ERC StG (G. B. contract number 714102) and Horizon2020 program, Innovative Training Network, ITN (G. B., eSCALED, contract number 765376) are gratefully acknowledged for funding. P.R.-M. and J.A.B. wish to thank the Max Planck Society for funding. Additionally, J.A.B. acknowledges funding from the Deutsche Forschungsgemeinschaft, DFG SPP1927 "Iron-Sulfur for Life: Cooperative Function of Iron-Sulfur Centers in Assembly, Biosynthesis, Catalysis, and Disease", Project BI 2198/1-1. P.R.-M. is supported financially by the European Research Council (ERC-2018-CoG BiocatSusChem 819580, to K.A. Vincent), and acknowledges Linacre College Oxford for her Junior Research Fellowship.

Funding Open access funding provided by Uppsala University.

Declarations

Conflict of interest The authors have no competing interests to declare that are relevant to the content of this article.

References

1. Madden C, Vaughn MD, Díez-Pérez I, Brown KA, King PW, Gust D, Moore AL, Moore TA (2012) J Am Chem Soc 134:1577–1582
2. Lubitz W, Ogata H, Rudiger O, Reijerse E (2014) Chem Rev 114:4081–4148
3. Hambourger M, Gervaldo M, Svedruzic D, King PW, Gust D, Ghirardi M, Moore AL, Moore TA (2008) J Am Chem Soc 130:2015–2022
4. Krishnan S, Armstrong FA (2012) Chem Sci 3:1015–1023
5. Plumeré N, Rüdiger O, Oughli AA, Williams R, Vivekananthan J, Pöller S, Schuhmann W, Lubitz W (2014) Nat Chem 6:822–827
6. Abe JO, Popoola API, Ajenifuja E, Popoola OM (2019) Int J Hydrogen Energy 44:15072–15086
7. Benoit SL, Maier RJ, Sawers RG, Greening C (2020) Microbiol Mol Biol Rev 84:e00092-e119
8. Esmieu C, Raleiras P, Berggren G (2018) Sustain Energy Fuels 2:724–750
9. Land H, Senger M, Berggren G, Stripp ST (2020) ACS Catal 10:7069–7086
10. Nangle SN, Sakimoto KK, Silver PA, Nocera DG (2017) Curr Opin Chem Biol 41:107–113
11. Simmons TR, Berggren G, Bacchi M, Fontecave M, Artero V (2014) Coord Chem Rev 270–271:127–150
12. Nicolet Y, Piras C, Legrand P, Hatchikian CE, Fontecilla-Camps JC (1999) Structure 7:13–23
13. Silakov A, Kamp C, Reijerse E, Happe T, Lubitz W (2009) Biochemistry 48:7780–7786
14. Berggren G, Adamska A, Lambertz C, Simmons TR, Esselborn J, Atta M, Gambarelli S, Mouesca JM, Reijerse E, Lubitz W, Happe T, Artero V, Fontecave M (2013) Nature 499:66–69
15. Peters JW, Lanzilotta WN, Lemon BJ, Seefeldt LC (1998) Science 282:1853–1858
16. Stripp ST, Goldet G, Brandmayr C, Sanganas O, Vincent KA, Haumann M, Armstrong FA, Happe T (2009) Proc Natl Acad Sci USA 106:17331–17336
17. Caserta G, Papini C, Adamska-Venkatesh A, Pecqueur L, Sommer C, Reijerse E, Lubitz W, Gauquelin C, Meynial-Salles I, Pramanik D, Artero V, Atta M, del Barrio M, Faivre B, Fourmond V, Léger C, Fontecave M (2018) J Am Chem Soc 140:5516–5526
18. Kubas A, Orain C, De Sancho D, Saujet L, Sensi M, Gauquelin C, Meynial-Salles I, Soucaille P, Bottin H, Baffert C, Fourmond V, Best RB, Blumberger J, Léger C (2017) Nat Chem 9:88–95
19. Morra S, Arizzi M, Valetti F, Gilardi G (2016) Biochemistry 55:5897–5900
20. Swanson KD, Ratzloff MW, Mulder DW, Artz JH, Ghose S, Hoffman A, White S, Zadvornyy OA, Broderick JB, Bothner B, King PW, Peters JW (2015) J Am Chem Soc 137:1809–1816
21. Esselborn J, Kertess L, Apfel U-P, Hofmann E, Happe T (2019) J Am Chem Soc 141:17721–17728
22. van der Westen HM, Mayhew SG, Veeger C (1978) FEBS Lett 86:122–126
23. Stiebritz MT, Reiher M (2012) Chem Sci 3:1739–1751
24. Glick BR, Martin WG, Martin SM (1980) Can J Microbiol 26:1214–1223
25. Patil DS, Moura JJ, He SH, Teixeira M, Prickril BC, DerVartanian DV, Peck HD, LeGall J, Huynh BH (1988) J Biol Chem 263:18732–18738
26. Kubas A, De Sancho D, Best RB, Blumberger J (2014) Angew Chem Int Ed 53:4081–4084
27. Albracht SPJ, Roseboom W, Hatchikian EC (2006) J Biol Inorg Chem 11:88–101
28. Pierik AJ, Hagen WR, Redeker JS, Wolbert RBG, Boersma M, Verhagen MFJM, Grande HJ, Veeger C, Mutsaers PHA, Sands RH, Dunham WR (1992) Eur J Biochem 209:63–72
29. Roseboom W, De Lacey AL, Fernandez VM, Hatchikian EC, Albracht SPJ (2006) J Biol Inorg Chem 11:102–118
30. Patil DS, He SH, Der Vartanian DV, Le Gall J, Huynh BH, Peck HD (1988) FEBS Lett 228:85–88
31. Kamp C, Silakov A, Winkler M, Reijerse EJ, Lubitz W, Happe T (2008) Biochim Biophys Acta. Bioenerg 1777:410–416
32. Bennett B, Lemon BJ, Peters JW (2000) Biochemistry 39:7455–7460
33. Rodríguez-Maciá P, Galle LM, Bjornsson R, Lorent C, Zebger I, Yoda Y, Cramer SP, DeBeer S, Span I, Birrell JA (2020) Angew Chem Int Ed 59:16786–16794
34. Rodríguez-Maciá P, Reijerse EJ, van Gastel M, DeBeer S, Lubitz W, Rüdiger O, Birrell JA (2018) J Am Chem Soc 140:9346–9350
35. Corrigan PS, Tirsch JL, Silakov A (2020) J Am Chem Soc 142:12409–12419
36. Mészáros LS, Ceccaldi P, Lorenzi M, Redman HJ, Pfitzner E, Heberle J, Senger M, Stripp ST, Berggren G (2020) Chem Sci 11:4608–4617
37. Land H, Ceccaldi P, Mészáros LS, Lorenzi M, Redman HJ, Senger M, Stripp ST, Berggren G (2019) Chem Sci 10:9941–9948
38. Meszaros LS, Nemeth B, Esmieu C, Ceccaldi P, Berggren G (2018) Angew Chem Int Ed 57:2596–2599
39. Khanna N, Esmieu C, Mészáros LS, Lindblad P, Berggren G (2017) Energy Environ Sci 10:1563–1567
40. Posewitz MC, King PW, Smolinski SL, Zhang L, Seibert M, Ghirardi ML (2004) J Biol Chem 279:25711–25720
41. Mulder DW, Ortillo DO, Gardenghi DJ, Naumov AV, Ruebush SS, Szilagyi RK, Huynh B, Broderick JB, Peters JW (2009) Biochemistry 48:6240–6248
42. Mulder DW, Boyd ES, Sarma R, Lange RK, Endrizzi JA, Broderick JB, Peters JW (2010) Nature 465:248–251
43. Wegelius A, Khanna N, Esmieu C, Barone GD, Pinto F, Tamagnini P, Berggren G, Lindblad P (2018) Energy Environ Sci 11:3163–3167
44. Birrell JA, Wrede K, Pawlak K, Rodriguez-Maciá P, Rüdiger O, Reijerse EJ, Lubitz W (2016) Isr J Chem 56:852–863
45. Rodríguez-Maciá P, Pawlak K, Rüdiger O, Reijerse EJ, Lubitz W, Birrell JA (2017) J Am Chem Soc 139:15122–15134
46. Goldet G, Brandmayr C, Stripp ST, Happe T, Cavazza C, Fontecilla-Camps JC, Armstrong FA (2009) J Am Chem Soc 131:14979–14989
47. Lempp M, Lubrano P, Bange G, Link H (2020) Biol Chem 401:1479–1485
48. Adamska-Venkatesh A, Krawietz D, Siebel J, Weber K, Happe T, Reijerse E, Lubitz W (2014) J Am Chem Soc 136:11339–11346
49. Esselborn J, Lambertz C, Adamska-Venkatesh A, Simmons T, Berggren G, Noth J, Siebel J, Hemschemeier A, Artero V, Reijerse E, Fontecave M, Lubitz W, Happe T (2013) Nat Chem Biol 9:607–609
50. Knörzer P, Silakov A, Foster CE, Armstrong FA, Lubitz W, Happe T (2012) J Biol Chem 287:1489–1499
51. Mulder DW, Guo Y, Ratzloff MW, King PW (2017) J Am Chem Soc 139:83–86
52. Mulder DW, Ratzloff MW, Bruschi M, Greco C, Koonce E, Peters JW, King PW (2014) J Am Chem Soc 136:15394–15402
53. Wegelius A, Land H, Berggren G, Lindblad P (2021) Cell Rep Phys Sci 2:100376
54. Duan J, Mebs S, Laun K, Wittkamp F, Heberle J, Happe T, Hofmann E, Apfel U-P, Winkler M, Senger M, Haumann M, Stripp ST (2019) ACS Catal 9:9140–9149

55. Le Cloirec A, Davies SC, Evans DJ, Hughes DL, Pickett CJ, Best SP, Borg S (1999) ChemComm 22:2285–2286
56. Lyon EJ, Georgakaki IP, Reibenspies JH, Darensbourg MY (1999) Angew Chem Int Ed 38:3178–3180
57. Schmidt M, Contakes SM, Rauchfuss TB (1999) J Am Chem Soc 121:9736–9737
58. Li H, Rauchfuss TB (2002) J Am Chem Soc 124:726–727
59. Fourmond V (2016) Anal Chem 88:5050–5052
60. Stoll S, Schweiger A (2006) J Magn Reson 178:42–55

Authors and Affiliations

Marco Lorenzi[1] · Pierre Ceccaldi[1,2] · Patricia Rodríguez-Maciá[3,4] · Holly Jayne Redman[1] · Afridi Zamader[1,5] · James A. Birrell[3] · Livia S. Mészáros[1] · Gustav Berggren[1]

Livia S. Mészáros
Livia.Meszaros@kemi.uu.se

[1] Molecular Biomimetics, Department of Chemistry–Ångström Laboratory, Uppsala University, Box 523, 75120 Uppsala, Sweden

[2] Present Address: Current Address: R&I Consultant, Home Office, Marseille, France

[3] Department of Inorganic Spectroscopy, Max Planck Institute for Chemical Energy Conversion, Stiftstrasse 34-36, 45470 Mülheim an der Ruhr, Germany

[4] Present Address: Current address: Department of Chemistry, Inorganic Chemistry Laboratory, University of Oxford, South Parks Road, Oxford OX1 3QR, UK

[5] Laboratoire de Chimie et Biologie des Métaux, Université Grenoble Alpes, CNRS, CEA, 17 rue des Martyrs, 38054 Grenoble, France